

Thickness dependence of spin Peltier effect visualized by thermal imaging technique

Shunsuke Daimon,^{1,2,3,*} Ken-ichi Uchida,^{4,5,6,†} Naomi Ujiie,⁷
Yasuyuki Hattori,⁷ Rei Tsuboi,¹ and Eiji Saitoh^{1,2,3,6,8}

¹*Institute for Materials Research, Tohoku University, Sendai 980-8577, Japan*

²*Advanced Institute for Materials Research, Tohoku University, Sendai 980-8577, Japan*

³*Department of Applied Physics, The University of Tokyo, Tokyo 113-8656, Japan*

⁴*National Institute for Materials Science, Tsukuba 305-0047, Japan*

⁵*Department of Mechanical Engineering, The University of Tokyo, Tokyo 113-8656, Japan*

⁶*Center for Spintronics Research Network, Tohoku University, Sendai 980-8577, Japan*

⁷*ALPS ALPINE CO., LTD., Tokyo 145-8501, Japan*

⁸*Advanced Science Research Center, Japan Atomic Energy Agency, Tokai 319-1195, Japan*

Magnon propagation length in a ferrimagnetic insulator yttrium-iron-garnet (YIG) has been investigated by measuring the YIG-thickness t_{YIG} dependence of the spin Peltier effect (SPE) in a Pt/YIG sample. We succeeded to measure the high-resolution t_{YIG} dependence of SPE by using the thermal imaging of SPE free from contamination by interference of infrared emissivity. Comparison between the experimental results and theoretical analyses demonstrates the existence of two propagation lengths for the magnon chemical potential and the magnon temperature.

PACS numbers: 72.20.Pa, 72.25.-b, 85.75.-d, 85.80.-b

I. INTRODUCTION

Interconversion between spin and heat currents has been extensively studied in the field of spin caloritronics [1,2]. The spin Peltier effect (SPE) [3–9], heat-current generation in response to spin-current injection, and the spin Seebeck effect (SSE) [10], spin-current generation in response to heat-current injection, are fundamental phenomena of the spin caloritronics. These phenomena have often been studied using metal/ferrimagnetic-insulator $\text{Y}_3\text{Fe}_5\text{O}_{12}$ (YIG) junction systems [3,4,6,10–14], where the spin and heat currents are carried by electron spins in the metal and magnons in YIG [15–17]. Since YIG shows a long magnon propagation length in the order of micrometers [6,12,13,16–19], it is favorable to utilize YIG for investigating a role of the magnons in the SPE and SSE.

One of the important parameters in spin caloritronics is the length scale of the SPE and SSE; these effects are characterized by length parameters, such as the magnon-spin diffusion length l_m and the magnon-phonon thermalization length l_{mp} [17,19,20]. These length parameters have been investigated by measuring discrete YIG-thickness t_{YIG} dependences of the SPE and SSE by preparing several YIG devices with different t_{YIG} [6,12,13,18,19]. These YIG films were prepared by the same growth technique in each experiment, such as liquid phase epitaxy (LPE) or sputtering. However, the devices contain variance of magnetic properties, such as a saturation magnetization and exchange stiffness constant, surface roughness, and crystallinity. These errors make it hard to analyze the fine t_{YIG} dependence and obtain correct values of the length parameters.

In this letter, we measured SPE by using a single Pt/YIG junction with a t_{YIG} gradient. The SPE in-

duces temperature change corresponding to the local t_{YIG} value, and we can extract the t_{YIG} dependence of the SPE in terms of a temperature distribution. The temperature change was detected via an infrared light emission from the sample by means of the lock-in thermography (LIT) [4]. The LIT method allows us to visualize the t_{YIG} dependence of the SPE in a single device. However, non-uniformity of the infrared emissivity contaminates the t_{YIG} dependence. We overcame this problem by measuring the SPE and emissivity distributions in the same sample. We succeeded to obtain the high-resolution t_{YIG} dependence of the SPE. Comparison between the experimental results and theoretical analyses confirms the existence of two propagation lengths l_m and l_{mp} for the SPE.

II. EXPERIMENTAL CONFIGURATION AND PROCEDURE

The SPE was measured for a Pt/YIG film with a gradient of the YIG thickness, ∇t_{YIG} [Fig. 1(a),(d)-(f)]. ∇t_{YIG} was introduced by obliquely polishing a single-crystalline YIG (111) film grown by LPE on a single-crystalline $\text{Gd}_3\text{Fe}_5\text{O}_{12}$ (GGG) (111) substrate. Since we introduced a gradual thickness change to a film with the size of $10 \times 10 \text{ mm}^2$, ∇t_{YIG} is almost uniform in the measurement range of 1 mm [Fig. 1(f)]. The value of ∇t_{YIG} along the y direction was obtained with a cross-sectional scanning electron microscope as $9.2 \mu\text{m}/\text{mm}$ [Fig. 1(f)]. After the polishing, a U-shaped Pt film with the thickness of 5 nm was sputtered on the surface of the YIG film. The longer lines of the U-shaped Pt were arranged parallel to the ∇t_{YIG} direction [Fig. 1(a),(d)]. In the microscope image of the Pt/YIG/GGG sample in Fig. 1(d), the yellow (gray) area above (below) the white dot-

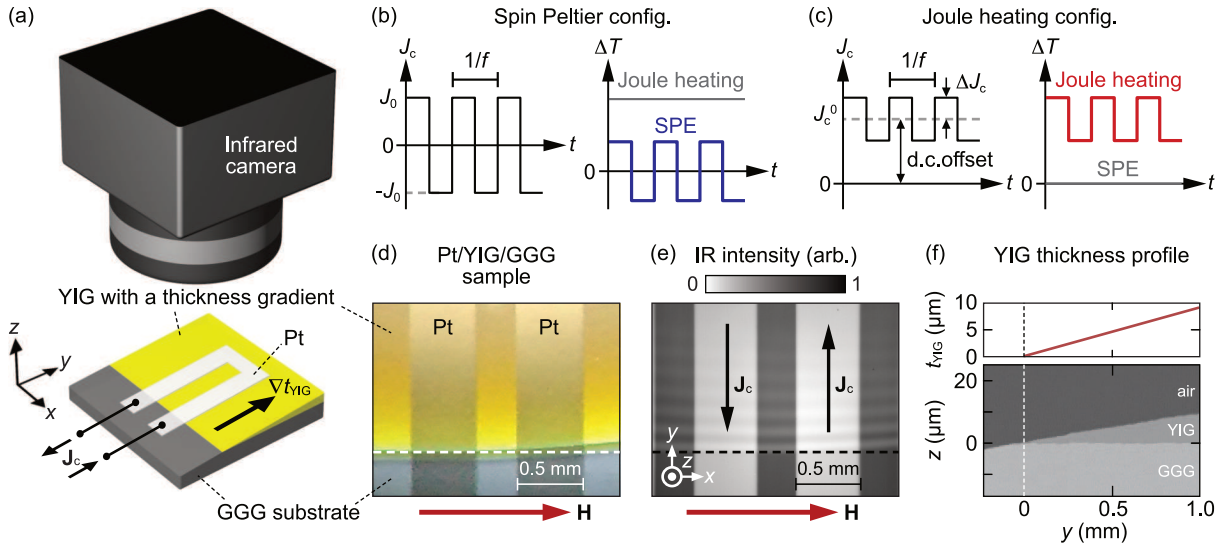


FIG. 1: (a) A schematic illustration of the SPE measurement using a Pt/YIG/GGG sample by means of the lock-in thermography method. A charge current, \mathbf{J}_c , is applied to the U-shaped Pt film fabricated on the YIG film with a thickness gradient, ∇t_{YIG} . (b),(c) Time t profile of an input a.c. charge current, J_c , and output temperature change, ΔT , for the (b) SPE and (c) Joule heating configurations. (d) An optical microscope image of the sample. The yellow (gray) area above (below) the white dotted line corresponds to the YIG film with ∇t_{YIG} (GGG substrate). \mathbf{H} is an applied magnetic field. (e) An infrared image of the sample. (f) A t_{YIG} profile and cross-sectional image of the sample obtained with a scanning electron microscope.

ted line corresponds to the YIG film with ∇t_{YIG} (GGG substrate).

The SPE induces temperature modulation in the Pt/YIG/GGG sample in response to charge-current injection to the Pt film. When we apply a charge current, \mathbf{J}_c , to the Pt film as shown in Fig. 1(a), a spin current is generated by the spin Hall effect in Pt [21,22] and induces spin accumulation in the Pt film close to the Pt/YIG interface [15]. The spin accumulation interacts with the magnetization, \mathbf{M} , in the YIG via the interfacial exchange coupling and induces a heat current across the Pt/YIG interface via the SPE. The heat current results in a temperature change, ΔT , which satisfies the following relation of the SPE [3,4]: $\Delta T = (\mathbf{J}_c \times \mathbf{M}) \cdot \mathbf{n}$, where \mathbf{n} is the normal vector of the Pt/YIG interface plane. Significantly, the temperature change induced by the SPE is localized around the Pt/YIG interface in length scale of micrometers owing to the formation of dipolar heat sources [4,6]. Therefore, the temperature change generated at each position on the YIG is not broadened within the scale of the spatial resolution of our infrared camera ($\sim 10 \mu\text{m}$). We can thus obtain local information of the spatial dependent SPE reflecting t_{YIG} at each position. The t_{YIG} resolution of our measurements is determined as 92 nm for the bare Pt/YIG/GGG sample by multiplying the t_{YIG} gradient and the spatial resolution of our infrared camera. Measurements were also performed using a black-ink-coated Pt/YIG/GGG sample to obtain the uniform infrared emission property of the sample. The surface of the sample was coated with insulating black ink with a thickness of 20 – 30 μm , which mainly con-

sists of SiZrO_4 , Cr_2O_3 , and iron oxide-based inorganic pigments [4,6]. Hereafter, we focus mainly on the bare Pt/YIG/GGG sample to obtain the precise thickness dependence of the SPE (note that the thick black-ink layer may reduce the spatial resolution of thermal images).

The t_{YIG} dependence of the SPE can be obtained by visualizing distribution of the temperature change by means of LIT [4,23–28]. A rectangular a.c. charge current, \mathbf{J}_c , with the amplitude J_0 (ΔJ_c), frequency f , and zero (non-zero) d.c. offset (J_c^0) was used as an input for the SPE (Joule heating) measurement [Fig. 1(b),(c)]. By extracting the first harmonic response of the temperature change in the SPE (Joule heating) configuration, we can detect the pure SPE (Joule heating) signal free from other thermal effects [4,6]. Here, the SPE induced temperature change ΔT_{1f} is defined as the component of ΔT oscillating in the same phase as \mathbf{J}_c because the SPE exactly follows the \mathbf{J}_c oscillation in the time scale of $1/f$ due to the quite fast response of the ΔT generated by the SPE [4,6,29,30]. In the LIT measurement, we obtain the first harmonic component of the infrared light emission ΔI_{1f} caused by ΔT_{1f} . By calibrating ΔI_{1f} to ΔT_{1f} using an infrared emissivity, ϵ , of the sample, we obtain the temperature change induced by the SPE [4,6]. All measurements of the SPE were performed under a magnetic field with a magnitude of 20 mT at room temperature and atmospheric pressure, where the magnetization of YIG aligns along the field direction at 20 mT.

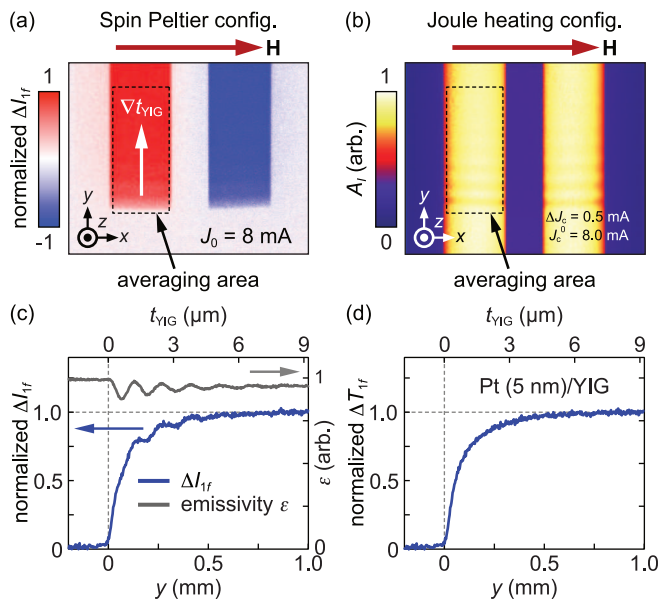


FIG. 2: (a) Lock-in signal of an infrared light emission ΔI_{1f} induced by the SPE. J_0 , \mathbf{H} , and ∇t_{YIG} are amplitude of the input charge current, an applied magnetic field, and the YIG-thickness gradient, respectively. (b) Lock-in amplitude of the infrared emission A_I induced by the Joule heating. (c), (d) Continuous YIG-thickness t_{YIG} dependence of (c) ΔI_{1f} and the emissivity ϵ and (d) the lock-in signal of the temperature change ΔT_{1f} induced by the SPE.

III. RESULTS AND DISCUSSION

Figure 2(a) shows the ΔI_{1f} signal from the Pt/YIG/GGG sample in the SPE configuration with $J_0 = 8$ mA and $f = 5$ Hz. The infrared signal appears only on the Pt/YIG structure but disappears on the Pt/GGG structure [compare Figs. 1(d) and 2(a)]. The sign of ΔI_{1f} is reversed when the charge current \mathbf{J}_c is reversed. These characteristics are consistent with the symmetry of the SPE and imply that the observed infrared signal comes from the SPE [3,4].

To focus on the t_{YIG} dependence of the SPE, the y dependence of the ΔI_{1f} values is plotted in Fig. 2(c), where the ΔI_{1f} values are averaged along the x direction in the area surrounded by the dotted line in Fig. 2(a). The ΔI_{1f} value gradually increases with small oscillation in the t_{YIG} dependence. The oscillation originates from the oscillation of the infrared emissivity ϵ of the sample due to multiple reflection of the infrared light in the YIG film [6]. To remove the oscillation in the t_{YIG} dependence of the SPE, ϵ was measured by the LIT with the Joule heating configuration with $\Delta J_c = 0.5$ mA, $f = 5$ Hz, and $J_c^0 = 8.0$ mA. Figure 2(b) shows an image of the amplitude of the infrared emission A_I induced by the Joule heating. Since the temperature change induced by the Joule heating is uniform on the Pt film, the A_I distribution on the Pt film solely depends on the ϵ distribution.

The t_{YIG} dependence of ϵ ($\propto A_I$) is plotted in Fig. 2(c), where the A_I values are averaged along the x direction in the same area as that for the SPE signal. We found that ϵ and ΔI_{1f} show the similar oscillating behavior. By calibrating ΔI_{1f} by ϵ , we obtained the t_{YIG} dependence of the temperature change ΔT_{1f} induced by the SPE [Fig. 2(d)]. The ΔT_{1f} value monotonically increases with increasing t_{YIG} .

We also measured the t_{YIG} dependence of the SPE in the black-ink/Pt/YIG/GGG sample [Fig. 3]. The sample with the black ink exhibits high and uniform emissivity without the spacial oscillation of ϵ appeared in the bare Pt/YIG/GGG sample [compare gray lines in Figs. 2(c) and 3(c),(d)]. In the SPE configuration with $J_0 = 8$ mA and $f = 5$ Hz, positive and negative ΔI_{1f} signals appear on the left and right Pt films, respectively [Fig. 3(b)]. By calibrating ΔI_{1f} with ϵ , we obtained the t_{YIG} dependence of the temperature change ΔT_{1f} induced by the SPE [Fig. 3(e)]. We found that ΔT_{1f} monotonically increases with increasing t_{YIG} even when the sample surface was coated with the black ink and the non-uniformity of the infrared light emissivity was removed.

The obtained t_{YIG} dependence cannot be explained by a simple exponential approximation used in the previous studies on the SPE and SSE [6,12,13,18]. Based on the simple assumption that the magnon diffuses in the YIG film with a magnon diffusion length l_m , the simple exponential approximation has been used for the analysis of the t_{YIG} dependence:

$$\Delta T \propto 1 - \exp(-t_{\text{YIG}}/l_m). \quad (1)$$

However, in general, this expression cannot be used for the small thickness region since the exponential function should be modulated by the boundary conditions for the spin and heat currents. In fact, when the experimental result is fitted by using Eq. (1), the fitting result shows significant discrepancy in small thickness regions $t_{\text{YIG}} < 4$ μm as shown in Fig. 4. The observed continuous t_{YIG} dependence of the SPE thus requires advanced understanding of the spin-heat conversion phenomena.

To discuss the t_{YIG} dependence of the SPE, some phenomenological theories are available. Here, we focus on two theories referenced in Refs. [17] and [31]. Following these theories, we calculate the t_{YIG} dependence of the SPE in the Pt/YIG/GGG system. The calculation was carried out by considering the following three processes: (i) spin current is generated by the SHE in Pt; (ii) the spin current is injected into YIG due to the interfacial exchange interaction; (iii) The spin current carries heat from Pt to YIG across the interface, and the resultant temperature distribution is calculated by solving diffusion equations for the spin and heat currents in the Pt/YIG system. The former two processes require the same calculation in the two theories, but the third process gives rise to different temperature changes in the different two theories due to the different heat-generation conditions. In the theory in Ref. [17], the authors assumed that the magnons in YIG locally fol-

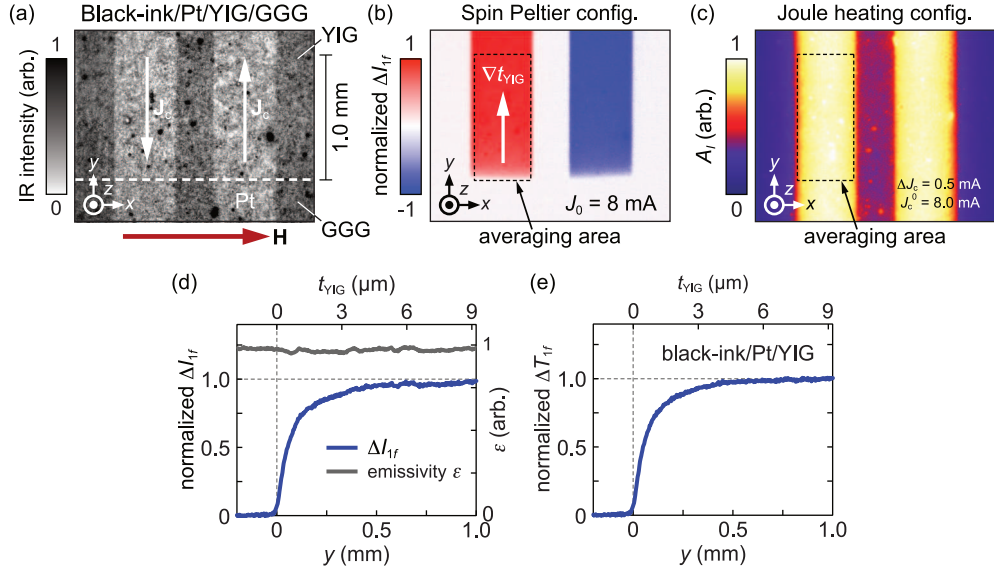


FIG. 3: (a) Infrared light image of a black-ink/Pt/YIG/GGG sample. \mathbf{J}_c and \mathbf{H} are a charge current applied to the Pt film and magnetic field, respectively. (b) Lock-in signal of an infrared light emission ΔI_{1f} induced by the SPE. J_0 and ∇t_{YIG} are amplitude of the input charge current and a YIG-thickness gradient, respectively. (c) Lock-in amplitude of an infrared light emission A_I induced by the Joule heating. ΔJ_c and J_c^0 denote the amplitude and a d.c. offset of the input charge current, respectively. (d),(e) Continuous YIG-thickness t_{YIG} dependence of (d) the ΔI_{1f} and the emissivity ϵ and (e) the lock-in signal of the temperature change ΔT_{1f} induced by the SPE.

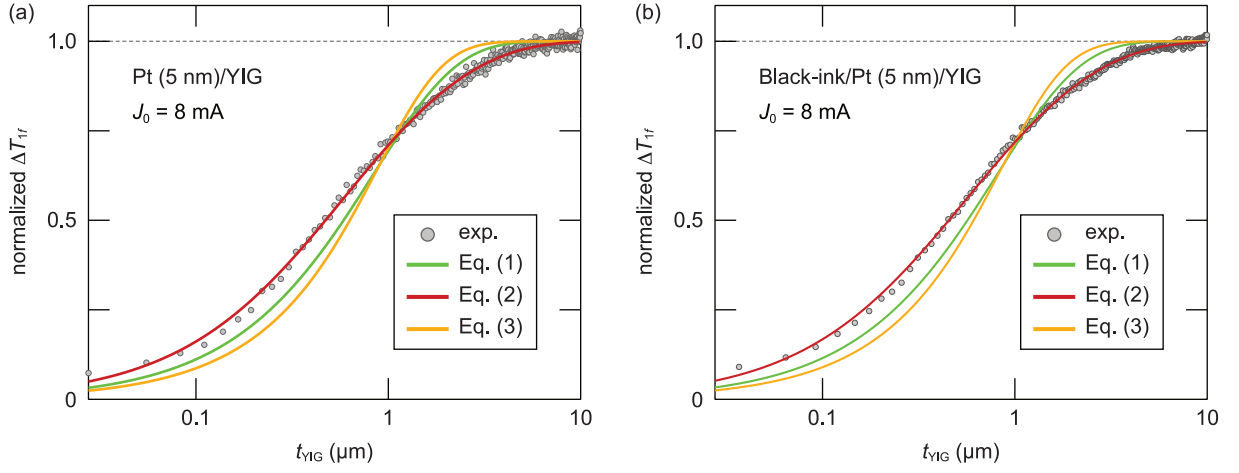


FIG. 4: Experimental results of the t_{YIG} dependence of the SPE for the (a) Pt/YIG/GGG and (b) black-ink/Pt/YIG/GGG samples and fitting curves using Eqs. (1)-(3).

low the Bose-Einstein distribution with μ_m and T_m [Fig. 5(a)]. The values of these parameters diffuse in the YIG following the Boltzmann and continuity equations, approximated into two diffusion equations: $\nabla^2 \mu_m = \mu_m / l_m^2$ and $\nabla^2 T_m = (T_m - T_p) / l_{\text{mp}}^2$, where T_p is the phonon temperature in YIG, and l_m and l_{mp} are the magnon-spin diffusion length and the magnon-phonon thermalization length, respectively [17]. The spin and heat currents carried by magnons are defined as $j_m \propto \nabla \mu_m$ and $j_{Q,m} \propto \nabla T_m$, respectively. These formalisms mean

that j_m and $j_{Q,m}$ are characterized by different diffusion lengths in YIG [Fig. 5(a)]. According to Ref. [17], l_m is much longer than l_{mp} due to the difference in scattering time scale of the magnon-conserving and magnon-non-conserving scattering processes. Under this assumption, heat current does not come to the YIG/GGG interface due to the short length scale of l_{mp} , and the temperature distribution generated by the SPE is not affected by t_{YIG} in the length scale of l_m , although the magnitude of ΔT is determined by spin current at the Pt/YIG interface,

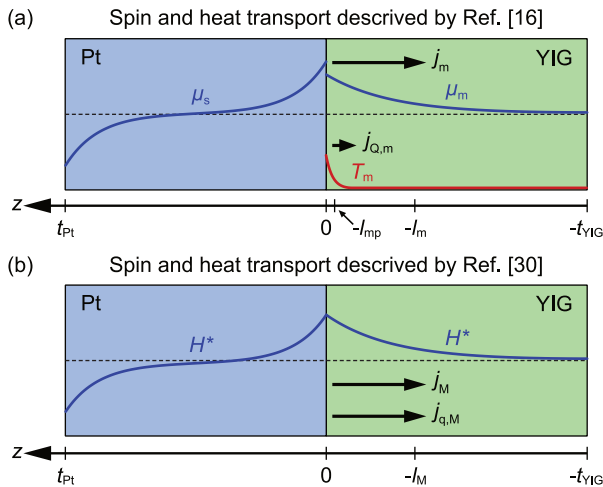


FIG. 5: (a) The calculation model for the SPE described in Ref. [17]. μ_s , μ_m , T_m , J_m , $J_{q,m}$, t_{Pt} , t_{YIG} , l_m , and l_{mp} are the spin accumulation, magnon chemical potential, magnon temperature, spin current, heat current carried by magnons, thickness of Pt and YIG, magnon diffusion length, and relaxation length for μ_m and T_m , respectively. (b) The calculation model for the SPE described in Ref. [31]. H^* , J_M , $J_{q,M}$, and l_M are the non-equilibrium component of the magnetic field, magnetization current, heat current carried by H^* , and diffusion length of H^* in YIG, respectively.

j_{int} . Then, by solving the above diffusion equations, we obtain the t_{YIG} dependence of ΔT (see Appendix section for more details):

$$\Delta T \propto j_{int} \propto \frac{1}{C \coth(t_{YIG}/l_m) - C + 1}, \quad (2)$$

where C is a t_{YIG} -independent constant used as a fitting parameter in our analysis. On the other hand, in Ref. [31], the authors proposed a theory based on non-equilibrium thermodynamics, where magnetization and heat currents are induced by a non-equilibrium component of the magnetic field H^* . H^* follows the diffusion equation $\nabla^2 H^* = H^*/l_M^2$, where l_M is a diffusion length [Fig. 5(b)]. The magnetization and heat currents are induced by the gradient of H^* and the local temperature T . The authors assumed that the heat current carried by magnons $j_{q,M}$ is proportional to the spin currents j_M : $j_{q,M} = \epsilon_M j_M$, where ϵ_M is the absolute thermomagnetic power coefficient [31]. Under the formalisms, the t_{YIG} dependence of the SPE is obtained by solving the above diffusion equation and a heat diffusion equation (see Appendix section for more details):

$$\Delta T \propto \frac{\cosh(t_{YIG}/l_m) - 1}{D \sinh(t_{YIG}/l_m) + (1 - D) \cosh(t_{YIG}/l_m)}, \quad (3)$$

where D is a t_{YIG} -independent constant used as a fitting parameter in our analysis.

Figure 4 shows the experimental results of the t_{YIG} dependence of the SPE and fitting curves based on Eqs. (2)

and (3). We found that Eq. (2) shows the best agreement with the experimental result and l_m is estimated to be $3.9 \mu\text{m}$ and $4.0 \mu\text{m}$ for the bare and black-ink-coated samples, respectively. In contrast, Eq. (3) cannot explain the experimental result in most thickness range $t_{YIG} < 4 \mu\text{m}$ and gives a shorter magnon diffusion length of $0.6 \mu\text{m}$ for both samples. Since the essential difference between the theories in Refs. [31] and [17] is whether the length scales of the spin and heat currents are same or not, these fitting results show that the spin and heat currents carried by magnons in YIG have different length scales, l_m and l_{mp} . Significantly, $l_m \gg l_{mp}$ is necessary for deriving Eq. (2). If $l_m \sim l_{mp}$, the theory in Ref. [17] gives t_{YIG} dependence written not in Eq. (2) but in Eq. (3), which cannot reproduce the experimental result. On the other hand, the theory in Ref. [17] can derive Eq. (2) by assuming that magnetization current flows much longer than that of magnetic heat current. Therefore, we conclude that spin current carried by magnons can flow much longer than that of heat current carried by magnons in YIG.

In the recent study on the SSE in Ref. [19], the authors reported non-monotonical increase of the SSE signal with t_{YIG} . Since the SSE signal takes a local maximum at $t_{YIG} \sim l_{mp}$, they estimated l_{mp} as 250 nm from the maximum point. However, in our Pt/YIG sample, the SPE signal monotonically increases with increasing t_{YIG} . These results suggest that l_{mp} is shorter than the t_{YIG} resolution of 60 nm for our YIG sample. The conclusion is consistent with the theoretical expectation $l_{mp} \sim 1 \text{ nm}$ [17].

IV. CONTINUOUS t_{YIG} DEPENDENCE OF THE SSE

To check the reciprocity between the SPE and SSE [32], we also measured the t_{YIG} dependence of the SSE by using a Pt/YIG/GGG sample with a t_{YIG} gradient. The YIG film used in the SSE measurement was not the same as that in the SPE measurements but it was obtained from the same YIG/GGG substrate. By obliquely polishing the surface of the YIG/GGG substrate, we obtained the YIG film with the t_{YIG} gradient of $12.2 \mu\text{m}/\text{mm}$ [Fig. 6(c)]. After the polishing, a Pt film with the thickness of 50 nm was sputtered on the surface of the YIG film [Figs. 6(a) and (d)]. Because magnetic properties of the YIG film was similar to these of the YIG film used in the SPE measurements, the reciprocity between the SPE and SSE can be checked by using the Pt/YIG/GGG sample.

To obtain the t_{YIG} dependence of the SSE, the SSE voltage was measured in the Pt/YIG/GGG sample by means of a micro-focused laser heating method [33–35]. As shown in Fig. 6(a), a laser with the wavelength of $1.3 \mu\text{m}$ and the diameter of the laser spot of $5.2 \mu\text{m}$ was focused on the sample surface to generate a spin current across the Pt/YIG interface. The spin current is converted into a charge current via the inverse spin Hall

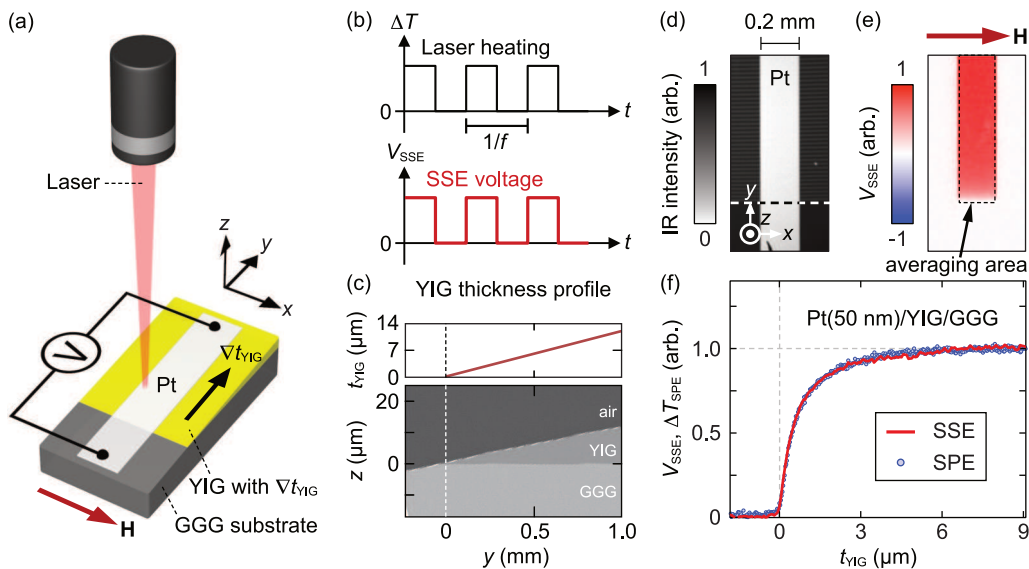


FIG. 6: (a) Schematic illustration of a SSE measurement using a laser heating method. We used a Pt/YIG/GGG sample with a YIG-thickness gradient ∇t_{YIG} . \mathbf{H} denotes an applied magnetic field. (b) Time t dependence of a temperature change of the sample ΔT and an output SSE voltage V_{SSE} induced by periodic irradiation of the laser light with frequency f . (c) t_{YIG} profile and cross-sectional image of the sample obtained by scanning electron microscope. (d) Infrared light image of the sample. (e) The SSE voltage V_{SSE} image induced by the laser heating. (f) Continuous YIG-thickness t_{YIG} dependence of V_{SSE} and comparison with that of the temperature change ΔT_{SPE} induced by the SPE.

effect in Pt [22] and was detected as an electrical voltage. While this method enabled the measurement of the local SSE voltage near the laser spot, the spatial resolution was larger than the laser spot size because the temperature gradient is broadened in the sample owing to the heat diffusion. To avoid the reduction in spatial resolution, we adopted a lock-in technique in the laser SSE measurement, where the laser intensity was modulated in a periodic square waveform with frequency $f = 5$ kHz and we measured the thermal voltage V_{1f} oscillating with the same frequency as that of the input laser [Fig. 6(b)]. This lock-in technique realized high spatial resolution for the SSE measurement because the heat diffusion cannot follow the oscillation of the laser intensity. Here, we defined the SSE voltage V_{SSE} as $[V_{1f}(+50 \text{ mT}) - V_{1f}(-50 \text{ mT})] / 2$ to remove magnetic-field-independent experimental artifacts. By scanning the position of the laser spot on the sample, we visualized the spatial distribution of the SSE voltage with high spatial resolution of $5.2 \mu\text{m}$.

Figure 6(e) shows the experimental results for the SSE measurement. In response to the laser heating, the clear voltage signal appeared in the Pt film. The t_{YIG} dependence of the SSE signal is plotted in Fig. 6(f), where the V_{SSE} values were averaged along the x direction in the area surrounded by the dotted line in Fig. 6(e). The SSE signal monotonically increases with increasing t_{YIG} . Significantly, the t_{YIG} dependence of the SSE demonstrated the same behavior as the SPE [Fig. 6(f)]. This result supports the reciprocity between the SPE and SSE and

strengthens our conclusion in the SPE measurements.

V. CONCLUSION

In conclusion, we revealed the length scale of the spin and heat transport by magnons in YIG by measuring the t_{YIG} dependence of the SPE in the Pt/YIG sample. This measurement was realized by using the YIG film with the t_{YIG} gradient and the LIT method, which allows us to obtain the continuous t_{YIG} dependence of the SPE in the single Pt/YIG sample. We found that the experimental result is well reproduced by assuming that the spin current flows much longer than that of the heat current carried by magnons in YIG. We also measured the t_{YIG} dependence of the SSE and found that the SPE and SSE demonstrate the same behavior in the t_{YIG} dependence. This understanding gives crucial information to understand the physical origin of the spin-heat conversion phenomena.

ACKNOWLEDGMENTS

The authors thank R. Iguchi, T. Kikkawa, M. Matsuo, Y. Ohnuma, and G. E. W. Bauer for valuable discussions. This work was supported by CREST “Creation of Innovative Core Technologies for Nano-enabled Thermal Management” (JPMJCR17I1), PRESTO “Phase Interfaces for Highly Efficient Energy Utilization” (JP-

MJPR12C1), and ERATO “Spin Quantum Rectification Project” (JPMJER1402) from JST, Japan, Grant-in-Aid for Scientific Research (A) (JP15H02012) and Grant-in-Aid for Scientific Research on Innovative Area “Nano Spin Conversion Science” (JP26103005) from JSPS KAKENHI, Japan, the Inter-University Cooperative Research Program of the Institute for Materials Research (17K0005), Tohoku University, and NEC Corporation.

APPENDIX: THEORETICAL DESCRIPTION OF t_{YIG} DEPENDENCE OF SPE

To analyze the t_{YIG} dependence of the SPE obtained from the experiments in the bare and black-ink-coated Pt/YIG/GGG samples, we introduced two phenomenological theories for the SPE, which can quantitatively derive its t_{YIG} dependence. Here, we considered a junction comprising a Pt film with a thickness of t_{Pt} , a YIG film with a thickness of t_{YIG} , and a GGG film with a thickness of t_{GGG} as illustrated in Figs. 5 and 7.

A. The t_{YIG} dependence of the SPE based on Ref. [17]

In Ref. [17] the authors formulated the SSE and SPE based on the Boltzmann theory for magnons in

a ferromagnetic insulator. In this formalism, the non-equilibrium distribution of the magnons (spins) in YIG (Pt) is described by the Bose-Einstein distribution with the magnon chemical-potential μ_{m} and magnon temperature T_{m} (the spin accumulation μ_{s} and electron temperature T_{e}) [Fig. 5(a)]. The authors derived that the spin and heat currents in YIG (Pt) are driven by the gradients of μ_{m} and T_{m} (μ_{s} and T_{e}), respectively, and constructed theories for the SSE and SPE.

In the YIG film, the linear-response relations for the magnon spin current j_{m} and heat current carried by magnons $j_{\text{Q,m}}$ are derived from the Boltzmann equation for the magnons [17]:

$$\begin{pmatrix} \frac{2e}{\hbar} j_{\text{m}} \\ j_{\text{Q,m}} \end{pmatrix} = - \begin{pmatrix} \sigma_{\text{m}} & L/T_{\text{p}} \\ \frac{\hbar}{2e} L & \kappa_{\text{m}} \end{pmatrix} \begin{pmatrix} \nabla_z \mu_{\text{m}} \\ \nabla_z T_{\text{m}} \end{pmatrix}, \quad (4)$$

where e , \hbar , σ_{m} , κ_{m} , L , and T_{p} are the electron charge, Planck constant, magnon spin conductivity, magnonic heat conductivity, bulk spin Seebeck coefficient, and phonon temperature, respectively. By combining these equations with the continuity equation for j_{m} and $j_{\text{Q,m}}$, the diffusion equations for μ_{m} and T_{m} can be derived [17]:

$$\begin{pmatrix} e & \alpha_{\mu} k_{\text{B}} \\ e\alpha_T/k_{\text{B}} & 1 \end{pmatrix} \begin{pmatrix} \nabla_z^2 \mu_{\text{m}} \\ \nabla_z^2 T_{\text{m}} \end{pmatrix} = \begin{pmatrix} e/l_{\text{m}}^2 & k_{\text{B}}/(l_{\rho T} T_{\text{p}}^2) \\ e/(k_{\text{B}} l_{\text{Q}\mu} \mu_{\text{m}}^2) & 1/l_{\text{mp}}^2 \end{pmatrix} \begin{pmatrix} \mu_{\text{m}} \\ T_{\text{m}} - T_{\text{p}} \end{pmatrix}, \quad (5)$$

where $\alpha_{\mu} = eL/(k_{\text{B}}\sigma_{\text{m}}T_{\text{p}})$ and $\alpha_T = \hbar k_{\text{B}}L/(2e\kappa_{\text{m}})$ are the measures for the relative ability of the chemical potential and temperature gradients to drive the spin current and magnon heat current, respectively. l_{m} , l_{mp} , $l_{\rho T} = l_{\text{m}}/\sqrt{\alpha_{\mu}}$, and $l_{\text{Q}\mu} = l_{\text{m}}/\sqrt{\alpha_T}$ are the magnon spin diffusion length, magnon-phonon relaxation length, magnon spin-heat relaxation length, and magnon heat-spin relaxation length, respectively. Here, we assumed that L is negligibly small: $\alpha_{\mu} \ll 1$ and $\alpha_T \ll 1$ [36]. Then, we obtained the simple diffusion equations:

$$\nabla_z^2 \mu_{\text{m}} = \mu_{\text{m}}/l_{\text{m}}^2, \quad (6)$$

$$\nabla_z^2 T_{\text{m}} = (T_{\text{m}} - T_{\text{p}})/l_{\text{mp}}^2. \quad (7)$$

Because Eq. (4) leads to $j_{\text{m}} \propto \nabla_z \mu_{\text{m}}$ and $j_{\text{Q,m}} \propto \nabla_z T_{\text{m}}$, these diffusion equations indicate that j_{m} and $j_{\text{Q,m}}$ diffuse in the length scales of l_{m} and l_{mp} , respectively. The authors claimed that l_{m} is much longer than l_{mp} owing to difference in time scale of the magnon-conserving and magnon-non-conserving scattering processes [17].

In the Pt film, the spin current j_{s} perpendicular to the

Pt/YIG interface and the charge current j_{c} flowing in the Pt film satisfy the following equation [17]:

$$\frac{2e}{\hbar} j_{\text{s}} = -\frac{\sigma_{\text{SH}}}{\sigma_{\text{e}}} j_{\text{c}} - \frac{\sigma'_{\text{e}}}{2} \nabla_x \mu_{\text{s}}, \quad (8)$$

where σ_{e} and σ_{SH} are the electrical conductivity and spin Hall conductivity, respectively. σ'_{e} is defined as $\sigma_{\text{e}} [1 - (\sigma_{\text{SH}}/\sigma_{\text{e}})^2]$. Here, we considered the relaxation-time approximation for the spin current: $\nabla_z (\frac{2e}{\hbar} j_{\text{s}}) = \mu_{\text{s}}/\tau_{\text{s}}$, where τ_{s} is the relaxation time. From these equations, the diffusion equation for μ_{s} can be derived:

$$\nabla_z^2 \mu_{\text{s}} = \mu_{\text{s}}/l_{\text{s}}^2, \quad (9)$$

where the spin diffusion length l_{s} is defined as $\sqrt{\sigma'_{\text{e}}\tau_{\text{s}}/2}$.

By using the above equations for the spin and heat currents, we calculated the temperature change ΔT_{SPE} induced by the SPE. In this formalism, because $l_{\text{mp}} \ll l_{\text{m}}$, the heat source generated in YIG by the SPE is confined in much shorter length scale than the magnon diffusion length of micrometers. Significantly, under this

assumption, the heat source distribution induced by the SPE is not affected by t_{YIG} when $t_{\text{YIG}} \gg l_{\text{mp}}$. In addition, the temperature distribution is also not affected by t_{YIG} when $t_{\text{YIG}} \gg l_{\text{mp}}$, because the temperature change in the Pt/YIG sample appears at the Pt/YIG interface due to the interfacial heat resistance as shown in Fig. 7(a) [4,6]. The SPE is only affected by the amplitude of the heat sources near the Pt/YIG interface, which is proportional to the spin current at the Pt/YIG interface j_{int} : $\Delta T_{\text{SPE}} \propto j_{\text{int}}$. To obtain j_{int} , we need

$$\left(\frac{2e}{\hbar} j_{\text{int}}\right) / \left(\frac{\sigma_{\text{SH}}}{\sigma_e} j_c\right) = \frac{2 \tanh\left(\frac{t_{\text{Pt}}}{2l_s}\right)}{\frac{\sigma'_e}{g_s l_s} - \coth\left(\frac{t_{\text{Pt}}}{2l_s}\right) - \tanh\left(\frac{t_{\text{Pt}}}{2l_s}\right) - \frac{\sigma'_e}{\sigma_m} \frac{l_m}{l_s} \coth\left(\frac{t_{\text{YIG}}}{l_m}\right)}. \quad (10)$$

Finally, from the proportional relation between ΔT_{SPE} and j_{int} , we obtained the temperature change generated by the SPE:

$$\Delta T_{\text{SPE}} \propto \frac{1}{C \coth(t_{\text{YIG}}/l_m) - C + 1}, \quad (11)$$

where C is a t_{YIG} -independent constant.

B. The t_{YIG} dependence of the SPE based on Ref. [31]

In Ref. [31], the authors formulated the SSE and SPE based on non-equilibrium thermodynamics. In this formalism, a non-equilibrium parameter in materials was described by a non-equilibrium component of the magnetic field defined as $H^* = H - H_{\text{eq}}$, where H and H_{eq} are the magnetic field and equilibrium magnetic field, respectively. The system is also characterized by the position-dependent temperature T . The authors derived that magnetization and heat currents are driven by the gradients of H^* and T and constructed theories for the SSE and SPE.

In the YIG film, the magnetization current j_{M} and heat current j_{q} are described by the following equation [31]:

$$\begin{pmatrix} j_{\text{M}} \\ j_{\text{q}} \end{pmatrix} = \begin{pmatrix} \sigma_{\text{M}} & \sigma_{\text{M}} \epsilon_{\text{M}} \\ \epsilon_{\text{M}} \sigma_{\text{M}} T & \kappa + \epsilon_{\text{M}}^2 \sigma_{\text{M}} T \end{pmatrix} \begin{pmatrix} \mu_0 \nabla_z H^* \\ -\nabla_z T \end{pmatrix}, \quad (12)$$

where σ_{M} , ϵ_{M} , and κ are the spin conductivity, absolute thermomagnetic power coefficient, and thermal conductivity, respectively. Notably, the heat current is divided into the non-magnetic heat current $j_{\text{q,NM}} = -\kappa \nabla_z T$ and the magnetic heat current $j_{\text{q,M}}$: $j_{\text{q}} = j_{\text{q,NM}} + j_{\text{q,M}}$. The authors assumed that $j_{\text{q,M}}$ is proportional to j_{M} with the proportionality factor of $\epsilon_{\text{M}} T$. In the case of the SPE,

to solve the diffusion equations [Eqs. (6),(9)]. As the boundary conditions for the diffusion equations, we assumed that the spin current does not flow at $z = t_{\text{Pt}}$ and $-t_{\text{YIG}}$, j_{s} and j_{m} are connected continuously at the Pt/YIG interface, and j_{int} is proportional to the difference between μ_{s} and μ_{m} at the Pt/YIG interface: $j_{\text{s}}(t_{\text{Pt}}) = 0$, $j_{\text{m}}(-t_{\text{YIG}}) = 0$, $j_{\text{s}}(+0) = j_{\text{m}}(-0)$, and $j_{\text{int}} = g_{\text{s}}[\mu_{\text{s}}(+0) - \mu_{\text{m}}(-0)]$ [17]. Under these boundary conditions, j_{int} is calculated by the following equation:

because the total heat generated by the SPE is zero, the continuity equation can be used: $\nabla j_{\text{q}} = 0$. In addition, because the system far from the Pt/YIG interface is a nearly equilibrium state, it can be assumed that the heat current vanishes at the end of the YIG $j_{\text{q}}(-t_{\text{YIG}}) = 0$. Under these conditions, the following simple equations can be derived:

$$\nabla_z T = j_{\text{M}} / (\hat{\epsilon}_{\text{M}} \hat{\sigma}_{\text{M}}), \quad (13)$$

$$j_{\text{M}} = \hat{\sigma}_{\text{M}} \mu_0 \nabla_z H^*, \quad (14)$$

where $\hat{\epsilon}_{\text{M}} = \epsilon_{\text{M}} \frac{\kappa + \kappa_{\text{M}}}{\kappa_{\text{M}}}$, $\hat{\sigma}_{\text{M}} = \sigma_{\text{M}} \frac{\kappa}{\kappa + \kappa_{\text{M}}}$, and $\kappa_{\text{M}} = \epsilon_{\text{M}}^2 \sigma_{\text{M}} T$. Here, we considered the relaxation-time approximation for the magnetization current: $\nabla_z j_{\text{M}} = H^* / \tau_{\text{YIG}}$, where τ_{YIG} is the relaxation time for YIG. From these equations, the diffusion equation for H^* can be derived:

$$\nabla_z^2 H^* = H^* / \hat{l}_{\text{YIG}}^2, \quad (15)$$

where $\hat{l}_{\text{YIG}} = \sqrt{\hat{\sigma}_{\text{M}} \mu_0 \tau_{\text{YIG}}}$.

In the Pt film, the magnetization current j_{M} perpendicular to the Pt/YIG interface and the charge current j_{e} flowing in the Pt film satisfy the following equation [31]:

$$j_{\text{M}} = -\theta_{\text{SH}} \left(\frac{\mu_{\text{B}}}{e}\right) j_{\text{e}} + \sigma'_{\text{M}} \mu_0 \nabla_z H^*, \quad (16)$$

where θ_{SH} , σ'_{PM} , μ_{B} , and e are the spin Hall angle, effective conductivity for the magnetization current, Bohr magneton, and elementary charge, respectively. Here, we considered the relaxation-time approximation for the magnetization current: $\nabla_z j_{\text{M}} = H^* / \tau_{\text{Pt}}$, where τ_{Pt} is the relaxation time. From these equations, the diffusion equation for H^* can be derived:

$$\nabla_z^2 H^* = H^* / l'_{\text{Pt}}{}^2, \quad (17)$$

where $l'_{\text{Pt}} = \sqrt{\hat{\sigma}_{\text{M}} \mu_0 \tau_{\text{Pt}}}$.

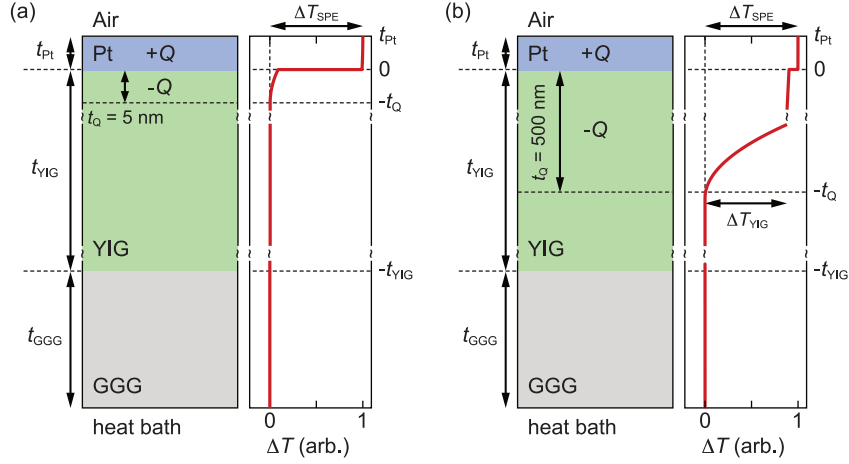


FIG. 7: Numerical simulations of the temperature change, ΔT , induced by dipolar heat sources in a one-dimensional model of a Pt/YIG/GGG junction. The bottom of the GGG substrate and top of the Pt film are in contact with the heat bath and air, respectively. As a simple model for the SPE, we set a dipolar heat source, $\pm Q$, near the Pt/YIG interface. The positive (negative) heat source $+Q$ ($-Q$) is uniformly placed in Pt (an area with a thickness, t_Q , in YIG). $t_{\text{Pt}} = 5 \mu\text{m}$, $t_{\text{YIG}} = 100 \mu\text{m}$, and $t_{\text{GGG}} = 500 \mu\text{m}$ are the thicknesses of Pt, YIG, and GGG, respectively. We set interfacial heat resistances to the Pt/YIG and YIG/GGG interfaces. The details of calculation conditions are mentioned in Refs. [4] and [6]. ΔT_{SPE} (ΔT_{YIG}) is defined as the temperature change between the top of Pt and bottom of GGG (the top and bottom of YIG). (a) Spatial profile of ΔT when t_Q is set to 5 nm, which corresponds to the physical picture derived from Ref. [17]. (b) Spatial profile of ΔT when t_Q is set to 500 nm, which corresponds to the physical picture derived from Ref. [31].

By using the above equations for the magnetization and heat currents, we calculated the temperature change ΔT_{SPE} induced by the SPE. In this formalism, because $j_{\text{q,M}}$ is proportional to j_{M} , the heat source generated in YIG by the SPE is broadened in the length scale of the magnon diffusion length of micrometers. In contrast, the heat source generated in Pt is confined in the thin Pt

film with the thickness t_{Pt} of 5 nm in our experiment. In this condition, the temperature change in the Pt/YIG sample practically appears in YIG [Fig. 7(b)]. Therefore, we assumed that $\Delta T_{\text{SPE}} \simeq \Delta T_{\text{YIG}}$, where T_{YIG} is the temperature change generated in the YIG film [see a numerical calculation result shown in Fig. 7(b)]. Then, we can calculate ΔT_{SPE} by the following equation:

$$\Delta T_{\text{SPE}} \simeq \Delta T_{\text{YIG}} = \int_{-t_{\text{YIG}}}^0 \nabla_z T(z) dz = \frac{1}{\hat{\epsilon}_{\text{M}} \hat{\sigma}_{\text{M}}} \int_{-t_{\text{YIG}}}^0 j_{\text{M}}(z) dz, \quad (18)$$

where Eq. (13) was used. To obtain j_{M} , we need to solve the diffusion equations [Eqs. (15),(17)]. As the boundary conditions for the diffusion equations, we assumed that the magnetization current does not flow zero at $z = t_{\text{Pt}}$ and $-t_{\text{YIG}}$, and H^* and j_{M} are continuous

at the Pt/YIG interface: $j_{\text{M}}(t_{\text{Pt}}) = 0$, $j_{\text{M}}(-t_{\text{YIG}}) = 0$, $H^*(+0) = H^*(-0)$, $j_{\text{M}}(+0) = j_{\text{M}}(-0)$. Under these boundary conditions, j_{M} is calculated as the following equation [31]:

$$j_{\text{M}}(z) = -j_0 \left[\sinh(z/\hat{l}_{\text{YIG}}) \coth(t_{\text{YIG}}/\hat{l}_{\text{YIG}}) - \cosh(z/\hat{l}_{\text{YIG}}) \right], \quad (19)$$

$$j_0 = j_{\text{MS}} \frac{\cosh(t_{\text{Pt}}/l'_{\text{Pt}}) - 1}{\cosh(t_{\text{Pt}}/l'_{\text{Pt}}) + r_{12} \sinh(t_{\text{Pt}}/l'_{\text{Pt}}) \coth(t_{\text{YIG}}/\hat{l}_{\text{YIG}})}, \quad (20)$$

$$j_{\text{MS}} = -\theta_{\text{SH}} \left(\frac{\mu_{\text{B}}}{e} \right) j_{\text{e}}, \quad (21)$$

where $r_{12} = (l'_{\text{PM}}\sigma'_{\text{PM}})/(\hat{l}_{\text{FI}}\hat{\sigma}_{\text{FI}})$. Finally, by substituting Eq. (19) in Eq. (18), we obtain the temperature change

generated by the SPE:

$$\Delta T_{\text{FI}} = \frac{[\cosh(t_{\text{Pt}}/l'_{\text{Pt}}) - 1] [\cosh(t_{\text{YIG}}/\hat{l}_{\text{YIG}}) - 1]}{\cosh(t_{\text{Pt}}/l'_{\text{Pt}}) \sinh(t_{\text{YIG}}/\hat{l}_{\text{YIG}}) + r_{12} \sinh(t_{\text{Pt}}/l'_{\text{Pt}}) \cosh(t_{\text{YIG}}/\hat{l}_{\text{YIG}})}, \quad (22)$$

$$\propto \frac{\cosh(t_{\text{YIG}}/\hat{l}_{\text{YIG}}) - 1}{D \sinh(t_{\text{YIG}}/\hat{l}_{\text{YIG}}) + (1 - D) \cosh(t_{\text{YIG}}/\hat{l}_{\text{YIG}})}, \quad (23)$$

where D is a t_{YIG} -independent constant. In the main

text, we replaced the symbol \hat{l}_{YIG} with l_{m} for simplicity.

* Electronic address: daimon@ap.t.u-tokyo.ac.jp

† Electronic address: UCHIDA.Kenichi@nims.go.jp

¹ G. E. W. Bauer, E. Saitoh, and B. J. van Wees, *Nat. Mater.* **11**, 391 (2012).

² S. R. Boona, R. C. Myers, and J. P. Heremans, *Energy Environ. Sci.* **7**, 885 (2014).

³ J. Flipse, F. K. Dejene, D. Wagenaar, G. E. W. Bauer, J. Ben Youssef, and B. J. van Wees, *Phys. Rev. Lett.* **113**, 027601 (2014).

⁴ S. Daimon, R. Iguchi, T. Hioki, E. Saitoh, and K. Uchida, *Nat. Commun.* **7**, 13754 (2016).

⁵ K. Uchida, R. Iguchi, S. Daimon, R. Ramos, A. Anadón, I. Lucas, P. A. Algarabel, L. Morellón, M. H. Aguirre, M. R. Ibarra, and E. Saitoh, *Phys. Rev. B* **95**, 184437 (2017).

⁶ S. Daimon, R. Iguchi, T. Hioki, K. Uchida, and E. Saitoh, *Phys. Rev. B* **96**, 024424 (2017).

⁷ Y. Ohnuma, M. Matsuo, and S. Maekawa, *Phys. Rev. B* **96**, 134412 (2017).

⁸ R. Iguchi, A. Yagmur, Y.-C. Lau, S. Daimon, E. Saitoh, M. Hayashi, and K. Uchida, *Phys. Rev. B* **98**, 014402 (2018).

⁹ K. Uchida, M. Sasaki, Y. Sakuraba, R. Iguchi, S. Daimon, E. Saitoh, and M. Goto, *Sci. Rep.* **8**, 16067 (2018).

¹⁰ K. Uchida, H. Adachi, T. Ota, H. Nakayama, S. Maekawa, and E. Saitoh, *Appl. Phys. Lett.* **97**, 172505 (2010).

¹¹ T. Kikkawa, K. Uchida, Y. Shiomi, Z. Qiu, D. Hou, D. Tian, H. Nakayama, X.-F. Jin, and E. Saitoh, *Phys. Rev. Lett.* **110**, 067207 (2013).

¹² T. Kikkawa, K. Uchida, S. Daimon, Z. Qiu, Y. Shiomi, and E. Saitoh, *Phys. Rev. B* **92**, 064413 (2015).

¹³ A. Kehlberger, U. Ritzmann, D. Hinzke, E.-J. Guo, J. Cramer, G. Jakob, M. C. Onbasli, D. H. Kim, C. A. Ross, M. B. Jungfleisch, B. Hillebrands, U. Nowak, and M. Kl'au, *Phys. Rev. Lett.* **115**, 096602 (2015).

¹⁴ R. Itoh, R. Iguchi, S. Daimon, K. Oyanagi, K. Uchida, and E. Saitoh, *Phys. Rev. B* **96**, 084422 (2017).

¹⁵ S. S.-L. Zhang and S. Zhang, *Phys. Rev. B* **86**, 214424 (2012).

¹⁶ S. M. Rezende, R. L. Rodríguez-Suárez, R. O. Cunha, A. R. Rodrigues, F. L. A. Machado, G. A. Fonseca Guerra, J. C. Lopez Ortiz, and A. Azevedo, *Phys. Rev. B* **89**, 014416 (2014).

¹⁷ L. J. Cornelissen, K. J. H. Peters, G. E. W. Bauer, R. A. Duine, and B. J. van Wees, *Phys. Rev. B* **94**, 014412 (2016).

¹⁸ E.-J. Guo, J. Cramer, A. Kehlberger, C. A. Ferguson, D. A. MacLaren, G. Jakob, and M. Kläui, *Phys. Rev. X* **6**, 031012 (2016).

¹⁹ A. Prakash, B. Flebus, J. Brangham, F. Yang, Y. Tserkovnyak, and J. P. Heremans, *Phys. Rev. B* **97**, 020408(R) (2018).

²⁰ B. Flebus, S. A. Bender, Y. Tserkovnyak, and R. A. Duine, *Phys. Rev. Lett.* **116**, 117201 (2016).

²¹ A. Hoffmann, *IEEE Trans. Magn.* **49**, 5172 (2013).

²² J. Sinova, S. O. Valenzuela, J. Wunderlich, C. H. Back, and T. Jungwirth, *Rev. Mod. Phys.* **87**, 1213 (2015).

²³ H. Straube, J.-M. Wagner, and O. Breitenstein, *Appl. Phys. Lett.* **95**, 052107 (2009).

²⁴ O. Breitenstein, W. Warta, and M. Langenkamp, *Lock-in Thermography: Basics and Use for Evaluating Electronic Devices and Materials* (Springer Science & Business Media, 2010).

²⁵ O. Wid, J. Bauer, A. Müller, O. Breitenstein, S. S. P. Parkin, and G. Schmidt, *Sci. Rep.* **6**, 28233 (2016).

²⁶ O. Wid, J. Bauer, A. Müller, O. Breitenstein, S. S. P. Parkin, and G. Schmidt, *J. Phys. D: Appl. Phys.* **50**, 134001 (2017).

²⁷ T. Seki, R. Iguchi, K. Takanashi, and K. Uchida, *Appl. Phys. Lett.* **112**, 152403 (2018).

²⁸ K. Uchida, S. Daimon, R. Iguchi, and E. Saitoh, *Nature* **558**, 95-99 (2018).

²⁹ R. Iguchi and K. Uchida, *Jpn. J. Appl. Phys.* **57**, 0902B6 (2018).

³⁰ A. Yagmur, R. Iguchi, S. Geprägs, A. Erb, S. Daimon, E. Saitoh, R. Gross, and K. Uchida, *J. Phys. D* **51**, 194002 (2018).

³¹ V. Basso, E. Ferraro, A. Magni, A. Sola, M. Kuepferling, and M. Pasquale, *Phys. Rev. B* **93**, 184421 (2016).

³² A. Sola, V. Basso, M. Kuepferling, C. Dubs, and M. Pasquale, *Sci. Rep.* **9**, 2047 (2019).

³³ M. Weiler, M. Althammer, F. D. Czeschka, H. Huebl, M. S. Wagner, M. Opel, I. Imort, G. Reiss, A. Thomas, R. Gross, and S. T. B. Goennenwein, *Phys. Rev. Lett.* **108**,

- 106602 (2012).
- ³⁴ N. Roschewsky, M. Schreier, A. Kamra, F. Schade, K. Ganzhorn, S. Meyer, H. Huebl, S. Geprägs, R. Gross, and S. T. B. Goennenwein, *Appl. Phys. Lett.* **104**, 202410 (2014).
- ³⁵ J. M. Bartell, C. L. Jermain, S. V. Aradhya, J. T. Brangham, F. Yang, D. C. Ralph, and G. D. Fuchs, *Phys. Rev. Appl.* **7**, 044004 (2017).
- ³⁶ $\alpha_\mu \ll 1$ and $\alpha_T \ll 1$ are not mentioned in Ref. [17]. However, these assumptions are necessary to explain their suggestion that $l_m \gg l_{mp}$. If $\alpha_\mu \sim 1$ and $\alpha_T \sim 1$, the relaxation lengths for the magnon spin current and magnon heat current take almost the same value owing to the off-diagonal term in the diffusion equations [Eq. (5)].